*29th EPS Conference on Plasma Phys. and Contr. Fusion Montreux, 17-21 June 2002 ECA Vol. **26B**, O-5.05 (2002)*

# Electromagnetic Gyrokinetic Microturbulence: Simulation and Visualization[1]

J. Candy and R.E. Waltz
*General Atomics, San Diego, CA*

**INTRODUCTION** Gyrokinetic simulation of tokamak transport has matured sufficiently to allow direct, *quantitative* comparison of numerical results with experimental data. It is to be emphasized that only with the simultaneous inclusion of many distinct and complex effects can this comparison realistically be made. The most important of these are:

1. nonlinear gyrokinetic ions and electrons (trapped and passing)
2. profile variation with sheared equilibrium $\mathbf{E} \times \mathbf{B}$ rotation (*i.e.*, finite-$\rho_*$ effects)
3. shaped plasma geometry (elongation, triangularity, etc.)
4. electron pitch-angle scattering
5. electromagnetic fluctuations, $\delta A_\parallel$, at finite plasma $\beta$

Item 2 defines what we will hereafter refer to as a *global* simulation. Above, $\rho_* \doteq \rho_s/a$ where $\rho_s$ is the ion-sound Larmor radius and $a$ is the plasma minor radius. We have carried out gyrokinetic simulations with the level of physical realism indicated by items 1-5. *Our first simulations reproduce not only the Bohm-like $\rho_*$-scaling observed in DIII-D L-mode discharges* [1], *but also match the actual values of the experimentally-inferred transport coefficients within a factor of two.* Although these results are preliminary, this is the first time a comprehensive gyrokinetic calculation has been successfully compared with experiment. It is only because of advances in numerical algorithms, steady increases in computing power, and years of microturbulence research, that this level of realism is possible. The cost of these simulations is extraordinary, however, with a single case taking 120 hours on 128 processors (IBM SP POWER3). Runs of this magnitude would have required roughly one year, and double the available memory, to complete on the largest Cray YMP machines of the early 1990s.

**THE NUMERICAL CHALLENGE** While electrostatic ion-temperature-gradient (ITG) turbulence with *adiabatic electrons* is relatively straightforward to simulate numerically, many researchers have found the coupled gyrokinetic simulation of electromagnetic turbulence to be a formidable challenge. The latter requires the simultaneous description of waves with different polarizations: the ITG mode (an electrostatic mode) for which $\delta A_\parallel \sim 0$, and the kinetic ballooning mode (KBM) for which $\delta E_\parallel \sim 0$. These modes are further modified by the presence of trapped electrons, which give rise to the trapped electron mode (TEM) of oscillation. Experience has shown that the KBM is the most difficult branch to describe gyrokinetically, because two terms in the Ampère equation, which are small in the limit $\beta_e \to 0$, are large and must cancel exactly when $\beta_e(m_i/m_e) > 1$. This cancellation is particularly problematic for particle-in-cell (PIC) codes, due to particle noise and interpolation error from the particle-to-field scattering operation. On the other hand, special differencing techniques can be devised in Eulerian codes to accurately recover the KBM branch [2, 3].

With the goal of making fully-realistic calculations of anomalous transport, we developed a new Eulerian gyrokinetic-Maxwell (GKM) code. This code, `gyro` [3], was designed from scratch to contain all the physics enumerated in the introduction. As such, it is the only global

[1]This is a report of work supported by the U.S. Department of Energy under Grant No. DE-FG03-95ER54309 and the Plasma Science Advanced Computing Initiative.

GKM solver that is also electromagnetic. Previously, we have used `gyro` to systematically demonstrate the mechanisms through which gyroBohm scaling (intrinsic to the flux-tube limit, $\rho_* \to 0$) can be broken [4]. The development of `gyro` was heavily influenced and continuously tested against the Eulerian flux-tube code `gs2` [5, 6]. Many algorithms were tried and rejected, and the final production version of `gyro` uses a variety of novel methods not found in other GKM solvers. The kinetic equation, for example, is not differenced in poloidal angle, but rather in *orbit-time* using high-order upwind schemes. This approach removes the singularity due to trapped particle bounce points. The fields are expanded in finite elements, and the Maxwell equations then solved with a Galerkin scheme. The full nonlinear collisionless dynamics are time-explicit and accurate to fourth-order in the timestep. The motivation for the latter approach was to eliminate nonlinear splitting errors, which we found to be unacceptably large in earlier versions of the code. Finally, collisions are treated in a semi-implicit fashion using operator splitting – with no viscous Courant limit on the timestep.

**DIII-D TRANSPORT SIMULATIONS** In this section, we describe simulations of DIII-D L-mode discharges 101381 and 101391 [1]. These are dimensionally-scaled shots which scan two values of $1/\rho_*$, namely 250 and 390. These values are quoted at an arbitrarily-chosen *reference radius*, $r_0/a = 0.6$. Also, in what follows, it will be useful to define the *gyroBohm* and *Bohm* scaling coefficients: $\chi_{\rm GB} \doteq \rho_* \chi_{\rm B}$ and $\chi_{\rm B} \doteq \rho_{\rm s} c_{\rm s}$, where $c_{\rm s}$ is the sound speed. Our explicit goal is to compute the various transport coefficients at the reference radius. The logic which dictates the choice of radial domain size is thus: it is sufficient to use a radial domain which covers only a fraction of the minor radius if, as the width of the radial domain is widened beyond this fraction, $\chi_i(r_0)$ is unchanged. For the discharges at hand, we find that $0.4 \le r/a \le 0.75$ is sufficient for a reasonable estimate of $\chi_i(r_0)$.

In Fig. 1a, we show a time-history of $\chi_i$ for a global ITG run with adiabatic electrons. This corresponds to DIII-D shot 101391, and includes full plasma shaping.

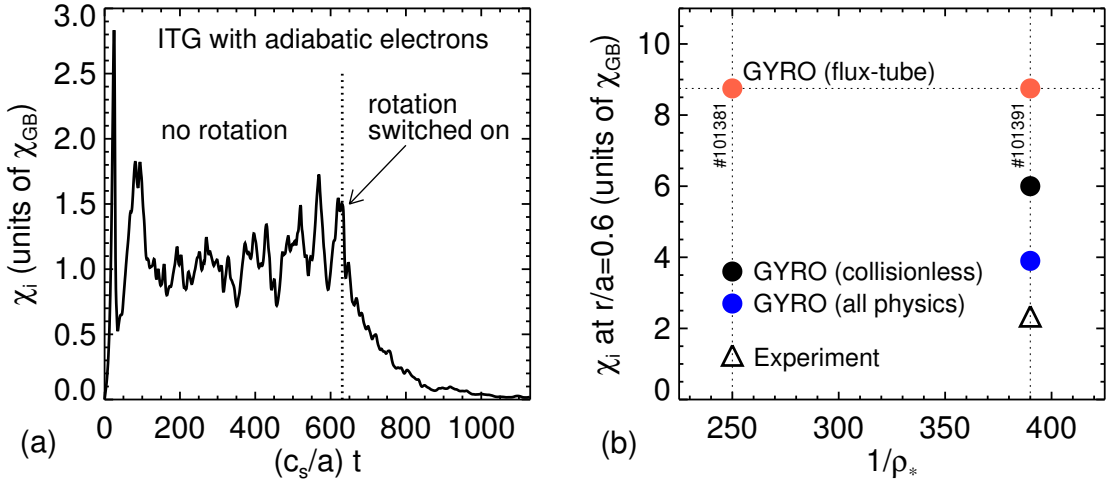


FIG. 1. `gyro` simulation data showing sensitivity of transport to different physics in discharges 101381 and 101391 ($1/\rho_* = 250$ and 390, respectively, at $r/a = 0.6$). Plot (a) shows $\chi_i$ from a global simulation of 101391 where electrons are taken to be adiabatic. The code is run to $(c_{\rm s}/a)t = 630$ with no equilibrium $\mathbf{E} \times \mathbf{B}$ rotational shear. Adding rotation leads to a complete quenching of the transport. Plot (b) shows a variety of simulations, all electromagnetic with kinetic electrons. A collisional flux-tube run (note the fixed gyroBohm scaling) largely overestimates the transport. Collisionless global runs with $\mathbf{E} \times \mathbf{B}$ shear do a better job. The final global simulations, with collisions and $\mathbf{E} \times \mathbf{B}$ shear, come encouragingly close to the experimental results in both cases.

Note that the adiabatic electron model, although it ignores all dynamical kinetic electron effects, has to date received by far the most attention in numerical simulation [7]. Interestingly, we find that the transport in Fig. 1a drops to zero when equilibrium $\mathbf{E}\times\mathbf{B}$ shear is included. This sheared rotation is known to be strongly stabilizing, and acts to entirely quench the transport. *This implies that kinetic electron physics is required for non-zero transport.* Fig. 1b summarizes a number of runs – all with kinetic electron dynamics. The most physically complete of these cases is a global, collisional electromagnetic simulation with equilibrium $\mathbf{E}\times\mathbf{B}$ shear and plasma flux-surface shape. The computed values of $\chi_i$ not only track the experimental trend, but give results which are impressively close in magnitude.

A more detailed look at the profiles of the energy (convection included) and particle diffusivities is given in Fig. 2. Because of the computational cost increases with the number of radial gridpoints, the runs presented here were carried out using relatively small radial box sizes (about $80\,\rho_i$ in both cases). In future work, we will attempt to assess in more detail the effect of widening the radial domain. With regard to additional physics, subsequent version of `gyro` are planned include a more detailed treatment impurity dynamics and ion-ion collisional effects.

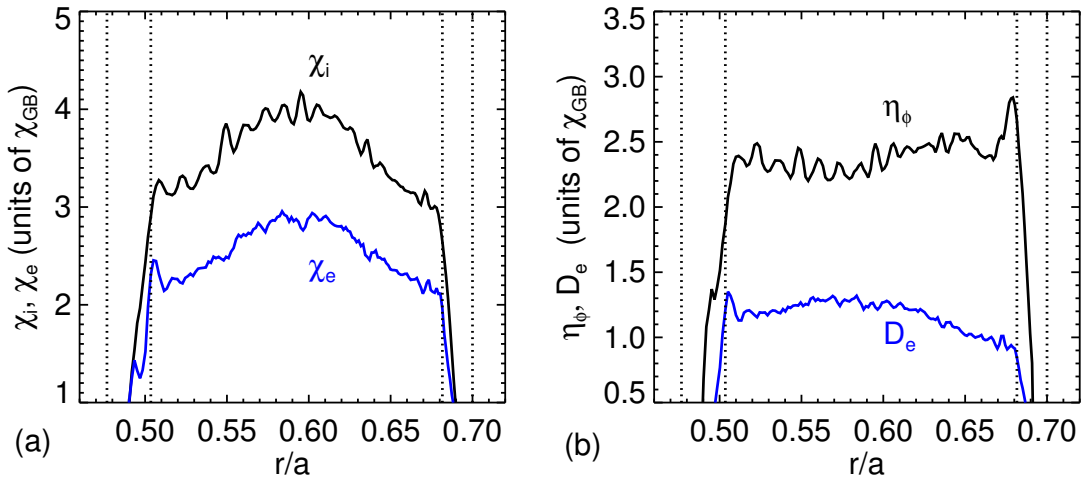


FIG. 2. Transport profiles, time-averaged over the interval $100 \le (c_s/a)t \le 450$ for discharge 101391. The energy-diffusivities, $\chi_i$ and $\chi_e$, are shown in (a), and the electron diffusivity, $D_e$, and toroidal viscosity (convection not included), $\eta_\phi$, are shown in (b). Vertical dotted lines denote the `gyro` multi-layer boundary regions. The fully-physical domain is the region $0.51 \le r/a \le 0.68$. We also compute, but do not show, the turbulent $e-i$ energy exchange.

Finally, the experimental and simulated values of $\chi_i$ at the reference radius are summarized in Table 1. We emphasize that flux-tube calculations *cannot differentiate these two discharges*, since they differ only by $\rho_*$.

| **SHOT** | $\chi_{GB}=\rho_s^2 c_s/a$ | $1/\rho_*$ | $\chi_i^{GYRO}/\chi_{GB}$ | $\chi_i^{exp}/\chi_{GB}$ |
|---|---|---|---|---|
| 101381 | $1.93\,m/s^2$ | 250 | 2.7 | 1.2 |
| 101391 | $1.02\,m/s^2$ | 385 | 3.9 | 2.3 |
| RATIO | | 0.65 | **0.69** | **0.52** |

TABLE 1. Comparison of numerical and experimental values of $\chi_i$ at $r/a=0.6$. $\chi$-ratios indicate closeness to gyroBohm (1.0) or Bohm (0.65) scaling. Thus, the simulation is (crudely speaking) nearly Bohm, while the experiment is slightly worse-than-Bohm.

The experiment, as is typical for L-mode discharges, gives a slightly worse-than-Bohm scaling of $\chi$ whereas `gyro` shows, roughly speaking, Bohm-like scaling.

**MICROTURBULENCE VISUALIZATION** The visualization and animation of data from microturbulence simulations continues to be a useful tool for communicating the physical content of complex numerical results to nonspecialists. In particular, through animation of `gyro` simulations, experimentalists have been able to clearly recognize (i) geodesic acoustic modes (GAMs), (ii) equilibrium sheared $\mathbf{E} \times \mathbf{B}$ rotation, (iii) linear structure of ballooning modes, (iv) nonlinear, self-generated $\mathbf{E} \times \mathbf{B}$ flows, and (v) development of radial "streamers". The visual impact of these results has led to increased confidence and interest in the more technical details. Animations and still images illustrating `gyro` results for a variety of different cases can be obtained from `http://web.gat.com/comp/parallel`. Fig. 3 shows one such still image.

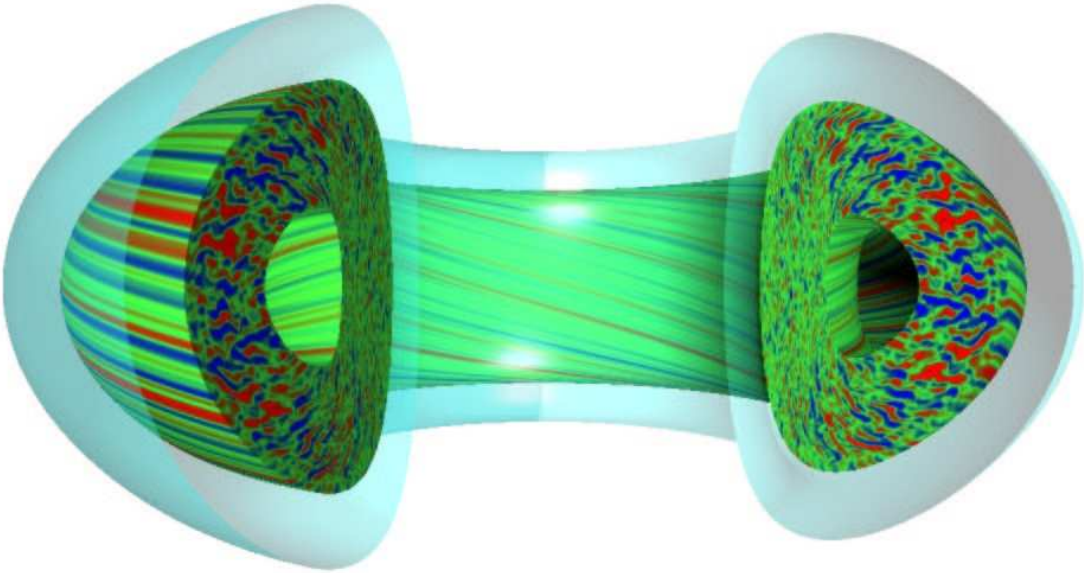

FIG. 3. Electrostatic potential isosurfaces for a strongly-shaped plasma, rendered using the Visualization Toolkit (VTK). The three-dimensional structure of turbulent fluctuations, highly elongated along field lines, is clearly illustrated. The blue halo shows the last closed flux surface.

## References

[1] G.R. McKee, C.C. Petty, R.E. Waltz, C. Fenzi, R.J. Fonck, J.E. Kinsey, T.C. Luce, and K.H. Burrell. *Nucl. Fusion* **41**, 1235 (2001).

[2] F. Jenko and W. Dorland. *Plasma Phys. Control. Fusion* **43**, A141 (2001).

[3] J. Candy and R.E. Waltz. General Atomics Report GA-A23876, to be published in J. Comput. Phys.

[4] R.E. Waltz, J. Candy, and M.N. Rosenbluth. *Phys. Plasmas* **9**, 1938 (2002).

[5] W. Dorland *et al.* in *Proc. 18th International Conference on Fusion Energy, Sorrento, Italy, 2000*. International Atomic Energy Agency, Vienna, paper TH2/5, in press.

[6] M. Kotschenreuther, G. Rewoldt, and W.M. Tang. *Comput. Phys. Commun.* **88**, 128 (1995).

[7] A.M. Dimits *et al. Phys. Plasmas* **7**, 969 (2000).